Artificial Noise Masked Microwave QR Code for Secure Vehicle Communications

Sai Xu, *Member, IEEE,* Yanan Du, *Member, IEEE,* and Jie Zhang, *Senior Member, IEEE*

***Abstract*—As a new paradigm, microwave quick response (QR) code has great potential to advance vehicle communications. However, its confidentiality issue still has to be resolved. For security, this correspondence proposes a scheme of artificial noise (AN)-masked microwave QR code, where a two-dimensional AN image is adopted to mask the QR code information on the reflection elements of intelligent reflecting surface as the information source (Alice). Meanwhile, a legitimate transceiver (Bob) transmits a radio frequency signal and then receives its echo signal to acquire the QR code information, in presence of a passive eavesdropper (Eve). To enhance the reception at Bob while degrading that at Eve, the transmitted signal and the AN mask are individually designed. The simulation results demonstrate the performance gain of the proposed scheme in terms of confidentiality.**

***Index Terms*—Microwave quick response code, physical layer security, artificial noise, intelligent reflecting surface, vehicle communications.**

I. Introduction

WITH evolution of intelligent transportation, it is self-evident that vehicle communications will play a vital role [1]. As a transformative paradigm, the emerging technology of microwave quick response (QR) code provides an excellent way to upgrade information interaction in vehicle-to-everything (V2X). For example, microwave QR code can be applied to realize the functions of identity authentication, electronic toll collection (ETC), etc. Compared to the conventional QR code, which has succeeded in mobile applications such as payment [2], microwave QR code operating in the microwave frequency band has some unique advantages, such as insensitivity to severe environmental conditions resulted from light intensity or block, large information capacity, etc.

The working principle of microwave QR code is to map the data message to an electromagnetic (EM)-sensitive metasurface in the form of QR code [3]. Once the EM wave strikes the metasurface, the message is modulated to the incident signal. With the signal reflected and received, the message of QR code can be conveyed. On the other hand, intelligent reflecting surface (IRS) [4], [5], owing to the adjustable amplitudes and phases of its elements, is a fantastic EM-sensitive metasurface for microwave QR code without doubt. By adopting one of various modulation schemes, such as phase shift keying (PSK), quadrature amplitude modulation (QAM), star-QAM, etc. [6]–[8], the message of QR code can be easily piggybacked on the elements of IRS. In essence, IRS-based microwave QR code is a specific implementation method of IRS backscatter communication, hence some related technologies can be found in many published works, such as [9], [10]

Currently, the technology of IRS-based microwave QR code is still on its initial stage. As a crucial aspect, its security issue deserves a thorough investigation [11]. By exploiting diversity of channels, physical-layer security (PLS) technologies are capable of securing wireless communications [12]. One of the key ideas of PLS is to leverage beamforming, relays, cooperative jamming, artificial noise (AN), etc. to strengthen the reception at the legitimate receiver while deteriorating that at the illegitimate one. For example, Liu *et al.* [13] considered IRS-aided multiple-input multiple-output multiple-antenna-eavesdropper (MIMOME) channels and minimized the secrecy outage probability by alternately optimizing the transmitting beamforming and the phase shifts of IRS. Wang *et al.* [14] investigated IRS-aided secure broadcasting in a millimeter wave symbiotic radio system, where the IRS realized its own information delivery when assisting secure broadcasting for the base station. Up to now, however, no studies have been done to secure IRS-based microwave QR code except for our previous work [11], where the transmitted signal at the legitimate receiver was utilized to jam the illegitimate receiver. Motivated by this fact, we attempt to improve the communication security of IRS-based microwave QR code from the perspective of superimposing an AN mask on the IRS.

This correspondence will focus on a secure communication system of AN-masked microwave QR code, where an IRS serves as an information medium to display a time-varying QR code masked by a two-dimensional AN image. Meanwhile, a legitimate transceiver transmits a radio frequency signal and then receives its echo signal to acquire the QR code information, in presence of a passive eavesdropper. Compared with existing communication schemes, AN and microwave QR code are produced together at the IRS end. Our main contributions are outlined as follows. 1) A secure communication system of AN-masked microwave QR code is modeled for the first time. 2) A feasible design scheme for transmitted signal and AN mask is proposed. 3) Simulations are conducted to demonstrate the performance gain of the proposed scheme in terms of confidentiality.

II. System Model

Fig. 1 shows a secure communication system of AN-masked microwave QR code, which comprises a legitimate transceiver

This work was supported in part by European Research Executive Agency's Horizon Europe MSCA 2022 Postdoctoral Fellowship CIRED under Grant (101109336); in part by European Commission's Horizon 2020 MSCA Individual Fellowship SICIS under Grant (101032170); in part by the National Natural Science Foundation of China (62101448); in part by Project funded by the China Postdoctoral Science Foundation (2022M722605).

Sai Xu, Yanan Du and Jie Zhang (e-mail: s.xu@sheffield.ac.uk; yanan.du@sheffield.ac.uk; jiliang.zhang@sheffield.ac.uk) are with the Department of Electronic and Electrical Engineering, University of Sheffield, Sheffield, S1 4ET, UK, (*Corresponding author*: Yanan Du)

Manuscript received XX XX, XXXX; revised XX XX, XXXX.

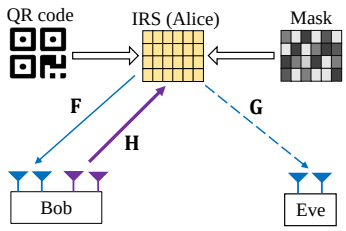

Fig. 1. An illustration of secure communication of AN-masked microwave QR code.

(Bob), a passive illegitimate receiver (Eve) and an information-carrying IRS (Alice)[1]. To be specific, the IRS serves as an information medium to display a time-varying QR code on its L EM-sensitive reflection elements. To enhance security, a two-dimensional AN image is also superimposed on the reflection elements of IRS to mask the QR code. With $N_{\rm t}$ transmitting and $N_{\rm r}$ receiving antennas equipped, Bob intends to obtain the QR code message from Alice by transmitting the EM wave and receiving its echo signal rebounded from the IRS. Meanwhile, Eve with $N_{\rm e}$ receiving antennas equipped also attempts to intercept and capture the reflected signal and decode the message from Alice. For linear decoding, $N_{\rm r}$ and $N_{\rm e}$ are both required to be no smaller than the number of reflection elements in a frequency band. Considering that the transmitted signal by Bob is used as an RF carrier signal and bears no information, the interference with itself and Eve can be reasonably ignored. It is assumed that all channels undergo quasi-static flat fading, and that the channel state information (CSI) of Bob is fully available while that of Eve is completely unknown.

When Bob emits an RF carrier signal towards the IRS, the echo signals received at Bob and Eve are respectively given by

$$\begin{aligned}\mathbf{y}_{\rm b} &= \mathbf{F}\boldsymbol{\Theta}\mathbf{H}\mathbf{x} + \mathbf{n}_{\rm b},\\ \mathbf{y}_{\rm e} &= \mathbf{G}\boldsymbol{\Theta}\mathbf{H}\mathbf{x} + \mathbf{n}_{\rm e},\end{aligned}$$

where $\mathbf{H} \in \mathbb{C}^{L\times N_{\rm t}}$, $\mathbf{F} \in \mathbb{C}^{N_{\rm r}\times L}$ and $\mathbf{G} \in \mathbb{C}^{N_{\rm e}\times L}$ denote the channels of Bob-Alice, Alice-Bob and Alice-Eve links, respectively. $\mathbf{x}$ denotes the transmitted signal by Bob. $\boldsymbol{\Theta}$ is the reflection coefficient matrix at the IRS. $\mathbf{n}_{\rm b}$ and $\mathbf{n}_{\rm e}$ are white Gaussian random vectors at Bob and Eve, with $\mathbf{n}_{\rm b} \sim (\mathbf{0}, \sigma_{\rm b}^2\mathbf{I})$ and $\mathbf{n}_{\rm e} \sim (\mathbf{0}, \sigma_{\rm e}^2\mathbf{I})$, respectively.

Since the pattern formed by the reflection coefficients of all IRS elements is composed of two parts: the QR code matrix $\mathbf{S}$ and the AN mask matrix $\mathbf{Z}$, we have $\boldsymbol{\Theta} = \mathbf{S} + \mathbf{Z}$. Let $\boldsymbol{\theta}$, $\mathbf{s}$ and $\mathbf{z}$ represent the vectors that consist of the diagonal elements of $\boldsymbol{\Theta}$, $\mathbf{S}$ and $\mathbf{Z}$, respectively. Mathematically, we have $\boldsymbol{\Theta} = {\rm diag}\{\boldsymbol{\theta}\}$, $\mathbf{S} = {\rm diag}\{\mathbf{s}\}$ and $\mathbf{Z} = {\rm diag}\{\mathbf{z}\}$. The signals received at Bob and Eve are respectively given by

$$\begin{aligned}\mathbf{y}_{\rm b} &= \mathbf{F}{\rm diag}\{\mathbf{H}\mathbf{x}\}\left(\mathbf{s}+\mathbf{z}\right) + \mathbf{n}_{\rm b},\\ \mathbf{y}_{\rm e} &= \mathbf{G}{\rm diag}\{\mathbf{H}\mathbf{x}\}\left(\mathbf{s}+\mathbf{z}\right) + \mathbf{n}_{\rm e}.\end{aligned}$$

Since the reflection coefficient of each IRS element is not greater than one, $|\mathbf{z}|_l = |\mathbf{s}+\mathbf{z}|_l \le 1$ holds with $l \in \mathcal{L} = \{1, 2, \cdots, L\}$. In view of the relationship $|\mathbf{s}|_l + |\mathbf{z}|_l \le 1 \Rightarrow |\mathbf{s}+\mathbf{z}|_l \le 1$, $|\mathbf{s}|_l \le \eta$ and $|\mathbf{z}|_l \le 1-\eta$ are used as the constraints of $\mathbf{s}$ and $\mathbf{z}$ with $0 \le \eta \le 1$, respectively, aiming to design the AN mask more easily.

At the IRS, each element can send one data stream by adjusting its complex-valued reflection coefficient to change the amplitude and phase of the incident signal. Mathematically, the process can be expressed as

$$\begin{aligned}\mathbf{F}{\rm diag}\{\mathbf{H}\mathbf{x}\}\mathbf{s} &= \sum_{l\in\mathcal{L}} \mathbf{F}{\rm diag}\{\mathbf{H}\mathbf{x}\}\mathbf{v}_l s_l = \sum_{l\in\mathcal{L}} \mathbf{F}{\rm diag}\{\mathbf{v}_l\}\mathbf{H}\mathbf{x}s_l,\\ \mathbf{G}{\rm diag}\{\mathbf{H}\mathbf{x}\}\mathbf{s} &= \sum_{l\in\mathcal{L}} \mathbf{G}{\rm diag}\{\mathbf{H}\mathbf{x}\}\mathbf{v}_l s_l = \sum_{l\in\mathcal{L}} \mathbf{G}{\rm diag}\{\mathbf{v}_l\}\mathbf{H}\mathbf{x}s_l,\end{aligned}$$

where $\mathbf{v}_l$ represents a vector whose elements are zero except that the l-th one is η. s_l denotes the information symbol of the l-th element of IRS. Letting $\mathbf{T}_{{\rm b},l} = \mathbf{F}{\rm diag}\{\mathbf{v}_l\}\mathbf{H}$ and $\mathbf{T}_{{\rm e},l} = \mathbf{G}{\rm diag}\{\mathbf{v}_l\}\mathbf{H}$, the signal-to-interference-plus-noise ratios (SINRs) at Bob and Eve for the l-th element are respectively given by

$$\begin{aligned}\gamma_{{\rm b},l} = \ & \mathbf{x}^H\mathbf{T}_{{\rm b},l}^H\Bigg[\sigma^2\mathbf{I} + \mathbf{F}{\rm diag}\{\mathbf{H}\mathbf{x}\}\mathbf{z}\mathbf{z}^H(\mathbf{F}{\rm diag}\{\mathbf{H}\mathbf{x}\})^H\\ &+ \sum_{l'\in\mathcal{L},l'\neq l}\mathbf{T}_{{\rm b},l'}\mathbf{x}\mathbf{x}^H\mathbf{T}_{{\rm b},l'}^H\Bigg]^{-1}\mathbf{T}_{{\rm b},l}\mathbf{x},\\ \gamma_{{\rm e},l} = \ & \mathbf{x}^H\mathbf{T}_{{\rm e},l}^H\Bigg[\sigma^2\mathbf{I} + \mathbf{G}{\rm diag}\{\mathbf{H}\mathbf{x}\}\mathbf{z}\mathbf{z}^H(\mathbf{G}{\rm diag}\{\mathbf{H}\mathbf{x}\})^H\\ &+ \sum_{l'\in\mathcal{L},l'\neq l}\mathbf{T}_{{\rm e},l'}\mathbf{x}\mathbf{x}^H\mathbf{T}_{{\rm e},l'}^H\Bigg]^{-1}\mathbf{T}_{{\rm e},l}\mathbf{x}.\end{aligned}$$

III. Design of Transmitted Signal and AN Mask

Given that the optimal design of transmitted signal and AN mask is a huge challenge, this section will present a feasible design scheme. Firstly, the transmitted signal is designed. Then, the AN mask is optimized.

A. Design of Transmitted Signal

Considering that the CSI of Bob is fully available while that of Eve is completely unknown, the signal vector $\mathbf{x}$ is transmitted towards the IRS. To focus most of the transmitted power on the IRS region with quasi-constant intensity on average, a half-wavelength spaced uniform planar array is adopted as the transmitting antennas at Bob. Let $N_{\rm t}^x$ and $N_{\rm t}^y$ denote the number of transmitting antennas along x-axis and y-axis, respectively, with $(x, y, 0)$ and $(0, 0, 0)$ being the positions of the $(n_{\rm t}^x, n_{\rm t}^y)$-th antenna and the $(1, 1)$-th one. Based on this, the beam pattern of the transmitting antennas at Bob is given by

$$g(\theta,\varphi) = \sum_{n_{\rm t}^y=1}^{N_{\rm t}^y}\sum_{n_{\rm t}^x=1}^{N_{\rm t}^x}\Phi\left(n_{\rm t}^x, n_{\rm t}^y\right)e^{-{\rm j}(x\theta+y\varphi)}, \qquad (1)$$

where $\Phi\left(n_{\rm t}^x, n_{\rm t}^y\right)$ denotes the weight factor of the $(n_{\rm t}^x, n_{\rm t}^y)$-th antenna for beamforming. θ and φ are given by $\theta = \frac{2\pi}{\lambda}\cos\vartheta_{\rm azi}\sin\vartheta_{\rm ele}$ and $\varphi = \frac{2\pi}{\lambda}\sin\vartheta_{\rm azi}\sin\vartheta_{\rm ele}$, where $\vartheta_{\rm azi}$

[1]The system design of AN-masked microwave QR code is different from AN-aided multiple-input multiple-output (MIMO) communications, as the IRS with the reflection constraint works as a passive QR code information source that is powered by Bob.

$$
\begin{aligned}
g(\theta,\varphi) &= \frac{d^2}{4\pi^2} e^{-\mathrm{j}(x\theta+y\varphi)} \sum_{n_{\mathrm{t}}^y=1}^{N_{\mathrm{t}}^y} \sum_{n_{\mathrm{t}}^x=1}^{N_{\mathrm{t}}^x} \int_{\frac{2\pi}{d}} \int_{\frac{2\pi}{d}} \omega(p,q) e^{\mathrm{j}(dpn_{\mathrm{t}}^x + dqn_{\mathrm{t}}^y)} \mathrm{d}p\mathrm{d}q \\
&= \frac{d^2}{4\pi^2} \int_{\frac{2\pi}{d}} \int_{\frac{2\pi}{d}} \omega(p,q) \sum_{n_{\mathrm{t}}^y=1}^{N_{\mathrm{t}}^y} e^{\mathrm{j}(dqn_{\mathrm{t}}^y - y\varphi)} \sum_{n_{\mathrm{t}}^x=1}^{N_{\mathrm{t}}^x} e^{\mathrm{j}(dpn_{\mathrm{t}}^x - x\theta)} \mathrm{d}p\mathrm{d}q \\
&= \frac{d^2 N_{\mathrm{t}}^x N_{\mathrm{t}}^y}{4\pi^2} e^{\mathrm{j}\frac{d(1-N_{\mathrm{t}}^x)}{2}\theta} e^{\mathrm{j}\frac{d(1-N_{\mathrm{t}}^y)}{2}\varphi} \int_{\frac{2\pi}{d}} \int_{\frac{2\pi}{d}} \omega'(p,q) \Xi_{N_{\mathrm{t}}^y}[d(q-\varphi)] \Xi_{N_{\mathrm{t}}^x}[d(p-\theta)] \mathrm{d}p\mathrm{d}q. \qquad (3)
\end{aligned}
$$

and ϑ_{ele} are the azimuth and elevation line-of-sight (LoS) angles of departure at Bob, respectively. The amplitude of $g(\theta,\varphi)$ can be employed to evaluate the signal intensity in the direction (θ,φ). Let $\Phi\left(n_{\mathrm{t}}^x, n_{\mathrm{t}}^y\right)$ denote the two-dimensional discrete signal in the spatial domain with the spatial sampling period equal to d in both the azimuth and elevation directions. According to the discrete-time Fourier transform (DTFT), $\Phi\left(n_{\mathrm{t}}^x, n_{\mathrm{t}}^y\right)$ can be rewritten as

$$
\Phi\left(n_{\mathrm{t}}^x, n_{\mathrm{t}}^y\right) = \frac{d^2}{4\pi^2} \int_{\frac{2\pi}{d}} \int_{\frac{2\pi}{d}} \omega(p,q) e^{\mathrm{j}(dpn_{\mathrm{t}}^x + dqn_{\mathrm{t}}^y)} \mathrm{d}p\mathrm{d}q, \quad (2)
$$

where $\int_{\frac{d}{2\pi}}(\cdot)\mathrm{d}(\cdot)$ is the integral in an arbitrary interval of length $\frac{d}{2\pi}$ and d denotes the space of adjacent transmitting antennas at Bob along the x-axis and y-axis directions. Moreover, $\omega(p,q)$ can be also given by

$$
\omega(p,q) = \sum_{n_{\mathrm{t}}^y=1}^{N_{\mathrm{t}}^y} \sum_{n_{\mathrm{t}}^x=1}^{N_{\mathrm{t}}^x} \Phi\left(n_{\mathrm{t}}^x, n_{\mathrm{t}}^y\right) e^{-\mathrm{j}(dpn_{\mathrm{t}}^x + dqn_{\mathrm{t}}^y)}.
$$

Substituting (2) into (1), $g(\theta,\varphi)$ is further given by (3) in the top of next page, where $\Xi(\cdot)$ denotes the Dirichlet kernel function and

$$
\omega'(p,q) = \omega(p,q) e^{\mathrm{j}\frac{(1+N_{\mathrm{t}}^x)}{2}dp} e^{\mathrm{j}\frac{(1+N_{\mathrm{t}}^y)}{2}dq}.
$$

Mathematically, $|g(\theta,\varphi)|$ is quasi-constant for $\theta_{\min} \le \theta \le \theta_{\max}$ and $\varphi_{\min} \le \varphi \le \varphi_{\max}$, but almost zero beyond this interval. Let

$$
\theta_{\min} \le p \le \theta_{\max}, \quad (4)
$$

$$
a < p < \theta_{\min} \text{ or } \theta_{\max} < p \le a + \frac{2\pi}{d}, \quad (5)
$$

$$
\varphi_{\min} \le q \le \varphi_{\max}, \quad (6)
$$

$$
b < q < \varphi_{\min} \text{ or } \varphi_{\max} < q \le b + \frac{2\pi}{d}, \quad (7)
$$

where a and b are two arbitrary numbers with satisfying $a < \theta_{\min}$, $a + \frac{2\pi}{d} > \theta_{\max}$, $b < \varphi_{\min}$ and $b + \frac{2\pi}{d} > \varphi_{\max}$. Then, the angular-domain coefficient for the focused region of the transmitted beam is designed as

$$
\omega(p,q) \propto \begin{cases} e^{-\mathrm{j}\frac{(1+N_{\mathrm{t}}^x)}{2}dp} e^{-\mathrm{j}\frac{(1+N_{\mathrm{t}}^y)}{2}dq}, \text{for (4) and (6)} \\ 0, \text{for (5) and (7).} \end{cases} \quad (8)
$$

Substituting (9) into (1), the beam pattern of the transmitting antennas at Bob is given by

$$
g(\theta,\varphi) \propto e^{\mathrm{j}\frac{d(1-N_{\mathrm{t}}^x)}{2}\theta} e^{\mathrm{j}\frac{d(1-N_{\mathrm{t}}^y)}{2}\varphi} \times \int_{\phi_{\min}}^{\phi_{\max}} \int_{\theta_{\min}}^{\theta_{\max}} \Xi_{N_{\mathrm{t}}^y}[d(q-\varphi)] \Xi_{N_{\mathrm{t}}^x}[d(p-\theta)] \mathrm{d}p\mathrm{d}q.
$$

The weight factor for beamforming can be calculated from (2), which yields

$$
\begin{aligned}
&\Phi\left(n_{\mathrm{t}}^x, n_{\mathrm{t}}^y\right) \propto \\
&\int_{\phi_{\min}}^{\phi_{\max}} \int_{\theta_{\min}}^{\theta_{\max}} e^{-\mathrm{j}\frac{(1+N_{\mathrm{t}}^y)}{2}dq} e^{-\mathrm{j}\frac{(1+N_{\mathrm{t}}^x)}{2}dp} e^{\mathrm{j}(dpn_{\mathrm{t}}^x + dqn_{\mathrm{t}}^y)} \mathrm{d}p\mathrm{d}q \\
&= \frac{e^{\mathrm{j}d\bar{n}_{\mathrm{t}}^x\theta_{\max}} - e^{\mathrm{j}d\bar{n}_{\mathrm{t}}^x\theta_{\min}}}{d\bar{n}_{\mathrm{t}}^x} \frac{e^{\mathrm{j}d\bar{n}_{\mathrm{t}}^y\varphi_{\max}} - e^{\mathrm{j}d\bar{n}_{\mathrm{t}}^y\varphi_{\min}}}{d\bar{n}_{\mathrm{t}}^y}, \qquad (9)
\end{aligned}
$$

where $\bar{n}_{\mathrm{t}}^x = n_{\mathrm{t}}^x - \frac{N_{\mathrm{t}}^x+1}{2}$ and $\bar{n}_{\mathrm{t}}^y = n_{\mathrm{t}}^y - \frac{N_{\mathrm{t}}^y+1}{2}$.

B. Design of AN Mask

Considering that the CSI of Bob is fully available while that of Eve is completely unknown, a common design is to place the AN mask vector $\mathbf{z}$ into the null space if $\mathbf{F}\mathrm{diag}\{\mathbf{H}\mathbf{x}\}$ is not a full-rank square matrix. Such a design can deteriorate the reception at Eve without any adverse impact on Bob. In the following, we will present a design scheme of AN mask vector. To be specific, $\mathbf{z}$ is optimized to maximize $\sum_{l\in\mathcal{L}} \log_2(1+\gamma_{\mathrm{b},l})$ under the constraint of $|\mathbf{z}|_l = 1-\eta$, which is formulated as

$$
\begin{aligned}
(\mathrm{P1}) \quad \max_{\mathbf{z}} \quad & \sum_{l\in\mathcal{L}} \log_2(1+\gamma_{\mathrm{b},l}), \\
s.t. \quad & \mathrm{C1}: |\mathbf{z}|_l = 1-\eta, l \in \mathcal{L}, \\
& \mathrm{C2}: 0 \le \eta \le 1.
\end{aligned}
$$

To address this problem, Lagrangian dual transform and quadratic transform are firstly employed to convert the objective function into a new form. Then, an alternate method is developed to optimize the problem. Specifically, using Lagrangian dual transform and quadratic transform, the objective function is equivalently transformed into

$$
\begin{aligned}
f(\alpha_{\mathrm{b},l}, \boldsymbol{\beta}_{\mathrm{b},l}, \mathbf{z}) = \max_{\alpha_{\mathrm{b},l}\ge 0} & \sum_{l\in\mathcal{L}} \left[\log_2(1+\alpha_{\mathrm{b},l}) - \alpha_{\mathrm{b},l}\right] \\
& + 2\sqrt{1+\alpha_{\mathrm{b},l}} \mathrm{Re}\{\boldsymbol{\beta}_{\mathrm{b},l}^H \mathrm{A}_{\mathrm{b},l}\} - \boldsymbol{\beta}_{\mathrm{b},l}^H \mathrm{B}_{\mathrm{b},l} \boldsymbol{\beta}_{\mathrm{b},l},
\end{aligned}
$$

where $\alpha_{\mathrm{b},l}$ is an auxiliary variable and $\boldsymbol{\beta}_{\mathrm{b},l}$ is an auxiliary variable vector, and

$$
\begin{aligned}
&\mathrm{A}_{\mathrm{b},l} = \mathbf{T}_{\mathrm{b},l}\mathbf{x}, \\
&\mathrm{B}_{\mathrm{b},l} = \sigma^2\mathbf{I} + \mathbf{U}\mathbf{z}\mathbf{z}^H\mathbf{U}^H + \sum_{l'\in\mathcal{L}} \mathbf{T}_{\mathrm{b},l'}\mathbf{x}\mathbf{x}^H\mathbf{T}_{\mathrm{b},l'}^H.
\end{aligned}
$$

Based on this, the problem can be solved by two alternate

Algorithm 1 The overall algorithm for designing transmitted signal and AN mask

1: **Initialization**: Set t = 0, ε, $f^{(0)}(\alpha_{\mathrm{b},l}, \boldsymbol{\beta}_{\mathrm{b},l}, \mathbf{z})$.
2: Adopt (9) to obtain $\Phi\left(n_{\mathrm{t}}^{x}, n_{\mathrm{t}}^{y}\right)$, followed by $\mathbf{x}$.
3: **repeat**
4: Set $t = t + 1$.
5: Adopt (10) and (11) to obtain $\alpha_{\mathrm{b},l}^{\circ}$ and $\boldsymbol{\beta}_{\mathrm{b},l}^{\circ}$.
6: Solve (P4) and employ rank-one recovery to obtain $\mathbf{z}^{\circ}$.
7: **until** $\frac{|f^{(t)}(\alpha_{\mathrm{b},l},\boldsymbol{\beta}_{\mathrm{b},l},\mathbf{z})-f^{(t-1)}(\alpha_{\mathrm{b},l},\boldsymbol{\beta}_{\mathrm{b},l},\mathbf{z})|}{f^{(t)}(\alpha_{\mathrm{b},l},\boldsymbol{\beta}_{\mathrm{b},l},\mathbf{z})} < \varepsilon$.
8: **return** $f^{(t)}(\alpha_{\mathrm{b},l}, \boldsymbol{\beta}_{\mathrm{b},l}, \mathbf{z})$.

steps. In the first step, the variables $\alpha_{\mathrm{b},l}$ and $\boldsymbol{\beta}_{\mathrm{b},l}$ are optimized with $\mathbf{z}$ fixed. In the second step, the variable $\mathbf{z}$ is optimized with $\alpha_{\mathrm{b},l}$ and $\boldsymbol{\beta}_{\mathrm{b},l}$ fixed.

Step-1) With $\mathbf{z}$ given, we can take the derivative to obtain the optimal $\alpha_{\mathrm{b},l}^{\circ}$ and $\boldsymbol{\beta}_{\mathrm{b},l}^{\circ}$. Mathematically, let

$$\frac{\partial f(\alpha_{\mathrm{b},l}, \boldsymbol{\beta}_{\mathrm{b},l}, \mathbf{z})}{\partial \alpha_{\mathrm{b},l}} = 0, \quad \frac{\partial f(\alpha_{\mathrm{b},l}, \boldsymbol{\beta}_{\mathrm{b},l}, \mathbf{z})}{\partial \boldsymbol{\beta}_{\mathrm{b},l}} = 0.$$

Then, it is deduced that the optimal $\alpha_{\mathrm{b},l}^{\circ}$ and $\boldsymbol{\beta}_{\mathrm{b},l}^{\circ}$ are given by

$$\alpha_{\mathrm{b},l}^{\circ} = \gamma_{\mathrm{b},l}, \tag{10}$$

$$\boldsymbol{\beta}_{\mathrm{b},l}^{\circ} = \sqrt{1+\alpha_{\mathrm{b},l}}\mathrm{B}_{\mathrm{b},l}^{-1}\mathrm{A}_{\mathrm{b},l}. \tag{11}$$

Step-2) With $\alpha_{\mathrm{b},l}$ and $\boldsymbol{\beta}_{\mathrm{b},l}$ given, the objective function is equivalent to

$$\max_{\mathbf{z}} \quad f(\alpha_{\mathrm{b},l}, \boldsymbol{\beta}_{\mathrm{b},l}, \mathbf{z}) \Longleftrightarrow \min_{\mathbf{z}} \quad \sum_{l\in\mathcal{L}} \boldsymbol{\beta}_{\mathrm{b},l}^{H}\mathbf{U}\mathbf{z}\mathbf{z}^{H}\mathbf{U}^{H}\boldsymbol{\beta}_{\mathrm{b},l}.$$

Then, the problem (P1) translates into

$$\begin{aligned} (\mathrm{P2}) \quad \min_{\mathbf{z}} \quad & \sum_{l\in\mathcal{L}} \boldsymbol{\beta}_{\mathrm{b},l}^{H}\mathbf{U}\mathbf{z}\mathbf{z}^{H}\mathbf{U}^{H}\boldsymbol{\beta}_{\mathrm{b},l}, \\ s.t. \quad & \mathrm{C1}, \mathrm{C2}. \end{aligned}$$

Defining $\bar{\mathbf{Z}} = \mathbf{z}\mathbf{z}^{H}$ and using semi-definite relaxation (SDR), the problem (P2) is reformulated as

$$\begin{aligned} (\mathrm{P3}) \quad \min_{\bar{\mathbf{Z}}} \quad & \mathrm{Tr}\left(\sum_{l\in\mathcal{L}} \mathbf{U}^{H}\boldsymbol{\beta}_{\mathrm{b},l}\boldsymbol{\beta}_{\mathrm{b},l}^{H}\mathbf{U}\bar{\mathbf{Z}}\right), \\ s.t. \quad & \mathrm{C2}: 0 \le \eta \le 1. \\ & \mathrm{C3}: \left[\bar{\mathbf{Z}}\right]_{l,l} = (1-\eta)^2, l \in \mathcal{L}, \\ & \mathrm{C4}: \bar{\mathbf{Z}} \succeq \mathbf{0}, \\ & \mathrm{C5}: \mathrm{rank}\left(\bar{\mathbf{Z}}\right) = 1. \end{aligned}$$

Ignoring the rank-one constraint C5, this problem is convex over $\bar{\mathbf{Z}}$ and easy to solve. According to its optimal solution $\bar{\mathbf{Z}}^{\circ}$, the rank-one solution $\mathbf{z}^{\circ}$ can be recovered by using singular value decomposition (SVD) or the Gaussian randomization method.

C. Computational Complexity Analysis

The procedure for designing the transmitted signal and AN mask is outlined in Algorithm 1. According to the interior-point method (IPM), the complexity of computing the problem (P3) is given by

$$C_{\mathrm{P3}} = \frac{\sqrt{3L}}{\epsilon}\left(8nL^3 + 4n^2L^2 + n^2L + nL\right).$$

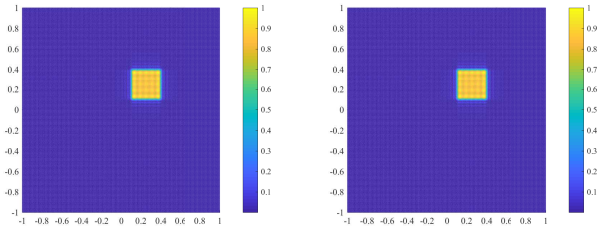

(a) Theoretical result (b) Simulation result

Fig. 2. An example of beam pattern, where $N_{\mathrm{t}}^{x} = N_{\mathrm{t}}^{y} = 64$, $d = \lambda/2$. The cut-off angles are $0.2 \le \frac{\lambda}{2\pi}\theta \le 0.4$ and $0.2 \le \frac{\lambda}{2\pi}\varphi \le 0.4$.

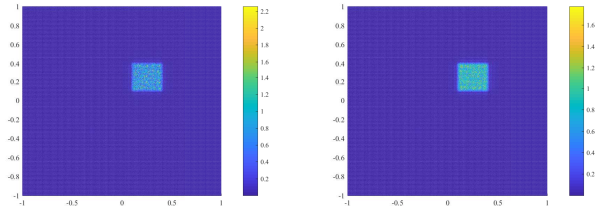

(a) κ = 0.5 (b) κ = 5

Fig. 3. The beam pattern on the IRS for the Rician channels with the Rician factor κ = 0.5 or 5, corresponding to the example of Fig. 2.

where $n = \mathcal{O}\left\{4L^2\right\}$ and ϵ denotes the accuracy until convergence.

IV. Numerical Results

This section will carry out numerical simulations to evaluate the security performance of the communication system of AN-masked microwave QR code. In simulations, the channels $\mathbf{H}$, $\mathbf{F}$ and $\mathbf{G}$ are generated by the Rician distribution with the Rician factor κ = 0.5 or 5. The transmission distances from Bob or Eve to Alice are both set as d = 20 m with the path loss PL $= -30 - 25\lg(d)$ dB. The noise variances σ_{b}^2 and σ_{e}^2 at Bob and Eve are both set as -90 dBW. The element number of IRS is set as $L = 64 \times 64$, which is equally divided into 8×64 different frequency-selective blocks each consisting of 8 elements. The number of transmitting antennas at Bob is set as $N_{\mathrm{t}} = 64 \times 64$. The numbers of receiving antennas at Bob and Eve are set as $N_{\mathrm{r}} = N_{\mathrm{e}} = 8$. Note that the number of receiving antennas is equal to that of IRS elements in a frequency band.

Figs. 2(a) and 2(b) depict the theoretical and simulation results for an example of beam pattern, where $N_{\mathrm{t}}^{x} = N_{\mathrm{t}}^{y} = 64$, d = $\lambda/2$. The cut-off angles are $0.2 \le \frac{\lambda}{2\pi}\theta \le 0.4$ and $0.2 \le \frac{\lambda}{2\pi}\varphi \le 0.4$. It is observed that the theoretical result is entirely consistent with the simulation one. According to the results, it is proved that most of the transmitted power from Bob can be focused on a small angular domain. Therefore, most of the transmitted power can shine on the IRS region with quasi-constant intensity on average, since all subchannels of the Rician channel $\mathbf{H}$ have the same value of expectation. This point can be verified by the simulations of Fig. 3, in which the Rician factor is set as κ = 0.5 or 5. In this observation, the transmitted power is restricted to a small region occupied by one of the IRS blocks with power fluctuation.

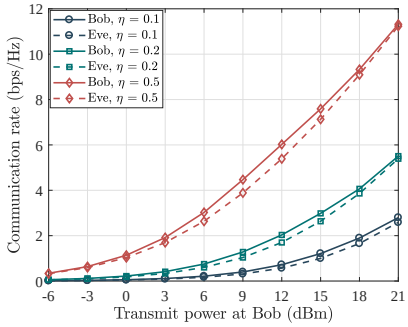

Fig. 4. Communication rate of Bob and Eve.

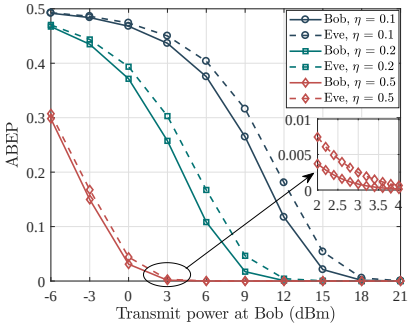

Fig. 5. ABEPs of Bob and Eve.

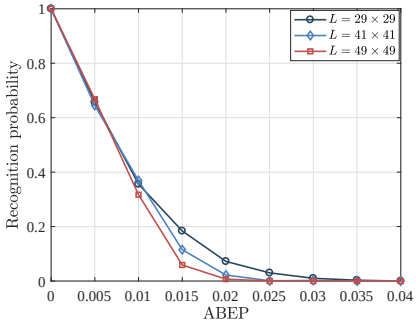

Fig. 6. Recognition probability of QR code *vs.* ABEP.

Fig. 4 shows the average communication rates of Bob and Eve for one IRS block, where the Rician factor is set as $\kappa = 0.5$ and it is assumed that 90% of the transmit power at Bob can be focused on one of the IRS blocks. In the simulations, iterative optimization and SDR are involved in Section III-B. According to a number of observations, it is found that the number of iteration until convergence is usually less than 15. Additionally, the optimal solution $\bar{\mathbf{Z}}^{\circ}$ is often a rank-one matrix, thus the eigenvector corresponding to its maximum eigenvalue is used approximately as the optimal vector solution $\mathbf{z}^{\circ}$. From Fig. 4, it is seen that the communication rates of Bob and Eve go up with the transmitted power at Bob increasing. Moreover, the communication rate of Bob is higher than Eve, which indicates that the considered system can achieve the security of the QR communication to a certain extent.

Fig. 5 shows how the transmit power at Bob affects the average bit error probabilities (ABEPs) at Bob and Eve with the modulation of BPSK considered. From Fig. 5, it is observed that the ABEPs at Bob and Eve decline until zero as the transmit power at Bob increases, and the ABEP gap between Bob and Eve firstly gets bigger but then becomes smaller. Fig. 6 depicts the relationship between the recognition probability of QR code and the ABEP. According to Figs. 5 and 6, the gap of recognition probability of QR code between Bob and Eve can be maximized by selecting the appropriate transmit power at Bob. Note that the ABEP for BPSK is obtained by using the formula of Shannon capacity to compute the equivalent SINR. Figs. 4, 5 and 6 imply that the QR code can be well recognized at Bob while being unrecognizable at Eve by adjusting the communication parameters.

V. Conclusions

This correspondence investigated a secure communication system of AN-masked microwave QR code. Based on the established system model, the transmitted signal and the AN mask were individually designed to enhance the security. According to the simulations, it can be concluded that: 1) Most of the transmitted power from Bob can be focused on a small region occupied by one of the IRS blocks by designing the transmitted signal. 2) The proposed scheme can achieve the security by realizing a larger average communication rate at Bob than Eve. 3) The QR code for communication can be well recognized at Bob while being unrecognizable at Eve by selecting the appropriate communication parameters.

References

[1] W. Duan, J. Gu, M. Wen, *et al.*, "Emerging technologies for 5G-IoV networks: Applications, trends and opportunities," *IEEE Netw.*, vol. 34, no. 5, pp. 283-289, Sept./Oct. 2020.

[2] G. Xue, Y. Li, H. Pan, *et al.*, "ScreenID: Enhancing QRCode security by utilizing screen dimming feature," *IEEE/ACM Trans. Netw.*, 2022, to be published, doi: 10.1109/TNET.2022.3203044.

[3] S. Xu, Y. Du, J. Zhang, *et al.*, "Microwave QR code: An IRS-based solution," *IEEE Trans. Veh. Technol.*, vol. 72, no. 5, pp. 6822-6826, May 2023.

[4] S. Gong, X. Lu, D. Hoang, *et al.*, "Toward smart wireless communications via intelligent reflecting surfaces: A contemporary survey," *IEEE Commun. Surveys Tuts.*, vol. 22, no. 4, pp. 2283-2314, 4th Quart 2020.

[5] M. Di Renzo, A. Zappone, M. Debbah, *et al.*, "Smart radio environments empowered by reconfigurable intelligent surfaces: How it works, state of research, and the road ahead," *IEEE J. Sel. Areas Commun.*, vol. 38, no. 11, pp. 2450-2525, Nov. 2020.

[6] M. Wu, X. Lei, X. Zhou, *et al.*, "Reconfigurable intelligent surface assisted spatial modulation for symbiotic radio," *IEEE Trans. Veh. Technol.*, vol. 70, no. 12, pp. 12918-12931, Dec. 2021.

[7] S. Guo, S. Lv, H. Zhang, *et al.*, "Reflecting modulation," *IEEE J. Sel. Areas Commun.*, vol. 38, no. 11, pp. 2548-2561, Nov. 2020.

[8] W. Tang, J. Dai, M. Chen, *et al.*, "MIMO transmission through reconfigurable intelligent surface: system design, analysis, and implementation," *IEEE J. Sel. Areas Commun.*, vol. 38, no. 11, pp. 2683-2699, Nov. 2020.

[9] S. Xu, C. Chen, Y. Du, *et al.*, "Intelligent reflecting rurface backscatter enabled uplink coordinated multi-cell MIMO network," *IEEE Trans. Wireless Commun.*, to be published, doi: 10.1109/TWC.2023.3236405.

[10] Y. -C. Liang, Q. Zhang, J. Wang, *et al.*, "Backscatter communication assisted by reconfigurable intelligent surfaces," *Proc. IEEE*, vol. 110, no. 9, pp. 1339-1357, Sept. 2022.

[11] Y. Du, S. Xu, K. Yu, *et al.*, "Communication security of microwave QR code," *IEEE Wireless Commun. Lett.*, to be published, doi: 10.1109/LWC.2023.3237252.

[12] Y. Liu, H. Chen, and L. Wang, "Physical layer security for next-generation wireless networks: Theories, technologies, and challenges," *IEEE Commun. Surv. Tut.*, vol. 19, no. 1, pp. 347-376, 1st Quart. 2017.

[13] Y. Liu, Z. Su, C. Zhang, *et al.*, "Minimization of secrecy outage probability in reconfigurable intelligent surface-assisted MIMOME system," *IEEE Trans. Wireless Commun.*, vol. 22, no. 2, pp. 1374-1387, Feb. 2023.

[14] C. Wang, Z. Li, T. -X. Zheng, *et al.*, "Intelligent reflecting surface-aided secure broadcasting in millimeter wave symbiotic radio networks," *IEEE Trans. Veh. Technol.*, vol. 70, no. 10, pp. 11050-11055, Oct. 2021.